Verification of Inverse Quench-Hardening Phenomena in Bearing Steel Specimens by Experiment and Computer Simulation

Kyozo Arimoto[1], **Chuanrong Jin**[2], **Shigeyuki Tamura**[2],

Kiyoshi Funatani[3], **Mamoru Tajima**[4]

1. Arimotech Ltd., Osaka, Japan
2. CRC Solutions Corp., Tokyo, Japan
3. IMST Inst., Nagoya, Japan
4. Kanagawa University, Kanagawa, Japan

Abstract: The appearance of lower hardness at the surface than at the core after through-hardening of steels is known as "inverse quench-hardening." Pioneering work was performed in the 1970s by establishing a simple test procedure where cylindrical specimens were cooled by air and brine sequentially to produce the effect. This phenomenon was described in relation to the polymer quenching and its effect to the improvement in the fatigue strength of the steel in the 1990s. The hardening mechanism in the same specimens as the pioneering work was recently examined using a finite element simulation method. However, this work has not been completed for lack of experimental quenching cooling curves for the comparisons. In this study, the same experiments using 20mm diameter cylindrical specimens as those of the pioneering work were conducted to obtain cooling curves and hardness distributions for comparing simulated results. Experimental cooling curves showed a temperature recovery as predicted by the simulation. Also the inverse quench-hardening phenomena were found in the measured and simulated hardness distributions of the specimens.

Key words: Inverse Quench-Hardening, Heat Treatment Simulation

TYPICALLY, steel parts show full-hardening throughout the cross-section or incomplete hardening at the core part depending on the hardenability of the steel. However, it was reported that some bearing steels with high hardenability occasionally exhibit lower hardness at the surface than at the core after oil quenching. This phenomenon was designated as "inverse quench-hardening" by Shimizu and Tamura [1], since the resulting hardness distributions were inverted from the conventional behavior.

Shimizu and Tamura [1, 2] developed a simplified experimental program using cylindrical specimens to analyze the inverse quench-hardening phenomenon occurring under the production conditions. The specimens were cooled by air and brine sequentially to produce the inverse hardening phenomenon. A theoretical explanation of inverse hardening in this specimen was also proposed, using a CCT diagram considering discontinuous cooling rates.

Liscic et al. [3, 4] reported inverse quench-hardening in their polymer quenching tests using AISI 4140 cylindrical specimens based on the Controllable Delayed Quenching (CDQ) technology. It was noted that this phenomenon contributes to the improvement in the fatigue strength based on their fatigue tests.

Arimoto et al. [5] simulated the experiments using cylindrical specimens conducted by Shimizu and Tamura [1, 2], and explained that the phenomenon is related to a pearlite transformation. The simulated results showed that a temperature recovery in the cooling curves during air-cooling was achieved by the generation of latent heat during the pearlitic transformation. However, they could not verify their simulated temperature recovery phenomena for lack of experimental cooling curves in the reports by Shimizu and Tamura [1, 2].

In this research, the same experimental procedure as performed by Shimizu and Tamura was used, and the cooling curves and hardness distributions on cross sections of the cylinders were measured. The cooling curves exhibited the same temperature recovery phenomenon that was predicted by the simulation during the air cooling. Moreover, the inverse quench-hardening phenomena were verified from the measured and simulated hardness distributions in the specimens after cooling.

1. Hardness Distributions in the Specimens

Shimizu and Tamura [1, 2] suggested that the practical inverse quench-hardening phenomenon occurring during oil quenching is due to the formation of the vapor blanket by the quenching oil. Lastly, a simplified experimental program was proposed to reproduce the phenomena in the laboratory by simulating the vapor blanket stage by air-cooling and using simple cylindrical specimens. Sizes of their cylindrical specimens were: 10, 15, 20, 25, 30, and 36 mm in diameter.

In this research, only the bearing steel specimen, 20 mm in diameter and 40 mm length, as shown in Fig. 1 was examined using the same experimental conditions as reported by Shimizu and Tamura. The chemical

Table 1 Composition (mass %) of Steel Specimen

Steel	C	Si	Mn	P	S	Cr
SUJ2	0.99	0.21	0.4	0.09	0.04	1.51

composition of the Japanese standard bearing steel, SUJ2, is shown in Table 1. The specimen was equipped three holes for thermo-couples at the positions of 0, 5 and 8 mm from the center of the cylinder as shown in Fig. 1 when measuring cooling curves.

After austenitizing at 840°C for 40 minutes, the specimens were initially cooled in air, and finally quenched in a 5% brine solution. In these tests, the influence of air-cooling on the inverse quench-hardening phenomenon was investigated by varying the cooling times from 60 to 120 s. In Fig. 2, solid curves show the measured hardness distributions in Rockwell C scale, HRC, on cross-sections of cylinders. The time shown adjacent to each curve indicates the time of air-cooling. A horizontal axis of the graph is the radial distance from the surface of the cylinder. The inverse quench-hardening phenomenon is found in the solid curves for 70 to 100 s times of air-cooling.

The hardness was measured at some points along the two straight lines that intersect each other at right angles at the center of the cylinder cross-section. This means that hardness data was measured at four points with an equal distance from the center. The solid curves in Fig.2 were drawn by the fitting of the average hardness at the four points. The dashed lines in Fig.2 show the hardness curves measured by Shimizu and Tamura [1]. In their experiment, the inverse quench-hardening phenomenon became remarkable at times from 50 to 90 s.

2. Simulation of the Inverse Quench-Hardening Phenomena

Since the simulation of the inverse quench-hardening phenomenon is mainly for predicting hardness, stress and distortion phenomena can be disregarded. The temperature field is therefore governed by the equation considering latent heat:
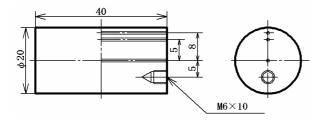
$$\rho c \dot{T} = \frac{\partial}{\partial x_i}\left(k\frac{\partial T}{\partial x_i}\right) + L_{IJ}\dot{\xi}_{IJ} \tag{1}$$

where T, ρ, c and k denote temperature, density, specific heat and thermal conductivity, respectively. $\dot{\xi}_{IJ}$ and L_{IJ} are phase transformation rate and latent heat produced from phase I to J transformation, respectively. In this research, the volume fraction of the diffusion type transformation, ξ_{IJ}, was estimated by the KJMA (Kolmogorov –Johnson –Mehl –Avrami) [6-8] equation:

$$\xi_{IJ} = 1 - \exp(-bt^n) \tag{2}$$

where b and n are material constants.

Agarwal et al. [9] studied temperature and volume fraction changes in cylinders under many cooling conditions by the simulation based on the eq. (1) and (2). Some of their simulated temperature changes were compared with the experiments by Takeo et al. [10], while the simulated transformation changes were reported without the comparison because of lack of the experimental data.

The research on the latent heat under transformations has been studied for many years, and especially the data of the latent heat in the A3 transformation of pure iron has been determined. Guillermet et al. [11] estimated the latent heat of pure iron strictly based on past experimental data and the thermodynamic model. However, there are few measurements on the latent heat of carbon steels, for example, carbon steels, containing 0.415, 0.435, 0.8, 0.84, and 1.22%C, by
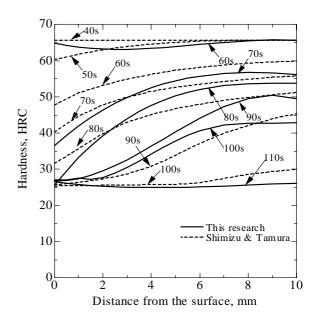

Fig.1 Test specimen Dimensions and Location of Instrumented Thermocouple Holes.

Fig.2 Measured Hardness Distribution in Specimens.

Table 2 Latent heat (kJ/kg) of pure iron and eutectoid steels

Authors	Pure Iron	Eutectoid steel (0.8%C)
Guillermet et al	18.1	
Awbery et al		43.0
Kramer et al		75.4-77.0
Krielaart et al		85 (cooling)
Tajima	16(heating), 19(cooling)	

Awbery et al. [12] and eutectoid steels by Kramer et al. [13]. The latent heat by Kramer et al. was measured using the method proposed by Smith [14].

Recently, the latent heat of carbon steels, containing 0.17, 0.36, 0.57, or 0.8%C, was measured by Krielaart et al. [15] using differential scanning calorimetry, DSC. Also, Tajima [16] applied DSC to ten carbon steels including with carbon contents of 0.001%C to 0.69%C.

Table 2 is a comparison of latent heat values in a pure iron and eutectoid steels from the above-mentioned experiments. The measured latent heats of the pure iron (0.001%C) by Tajima varied in the heating or cooling test, as shown in Table 2. The value of 18.1 kJ/kg by Guillermet et al. is between 16 and 19 kJ/kg determined by Tajima.

For the three eutectoid steels, the value by Awbery et al. is the lowest. The measurement of eutectoid steel by Kramer et al. showed a temperature arrest at the A1 transformation, while in the measurements by Krielaart et al. and Awbery et al., the temperature was changed continuously and not arrested. The measured values by Kramer et al. are between 75.4 and 77.0 kJ/kg, because of different pearlite spacing in the prepared specimens.

Since a diffusion-type transformation progresses over a wide range of temperatures under the usual heat treatment conditions, a temperature arrest does not occur during cooling. In this transformation process, it is assumed that the heat generation, which is calculated by multiplying whole latent heat L_{IJ} and transformation rate $\dot{\xi}_{IJ}$ as shown in eq. (1), is produced at each time increment. The accuracy of the model described by eq. (1) and (2) has not been rigorously evaluated, especially when producing temperature recoveries due to the latent heat.

3. Comparison between Experimental and Simulated Results

The inverse-quenching phenomena occurring in the test specimens of this research was simulated. We used the simulation software that was developed based on the finite element method for implementing the model described by eq. (1) and (2) and verified according to the procedure reported by Agarwal et al. [9].

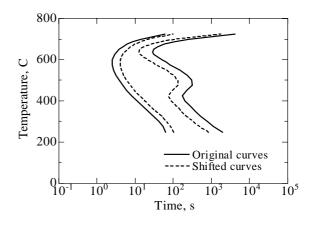The TTT diagram of the bearing steel was specified

Fig.3 Original and Shifted TTT Curves of 52100 Bearing Steel.

based on the data of 52100 steel, containing 1.02%C, 0.36%Mn, 0.2%Ni and 1.41%Cr, by US Steel [17]. However curves at the transformation start and end were shifted along the time-axis by trial and error as shown in Fig. 3. The performance of the transformation is affected by shifting the curves as explained by Arimoto et al. [5]. For the simulation, thermal physical properties were used from the data of BISRA [18] and/or calculated using the empirical formula by Miettinen [19]. A latent heat of 75.8 kJ/kg was applied for the austenite-pearlite transformation. This value was proposed by Kramer et al. [13], and used previously by Agarwal et al. [9] for their simulation. The heat transfer coefficient at the surface in the air-cooling was set based on the experimental data by Yamaguchi et al. [20].

The 20 mm cylindrical specimen was simulated as an axisymmetric problem using 100 finite elements along the radial axis. Simulated temperature changes during
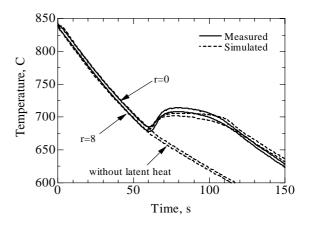

Fig.4 Measured and Simulated Cooling Curves during Air-cooling.
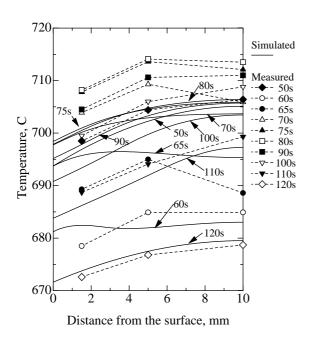
Fig.5   Measured   and   Simulated   Temperature
Distributions during Air-cooling.

air-cooling at two locations, 0 and 8 mm distances from
the center are shown by the solid curves in Fig. 4.
These curves agree with the dotted curves derived from
the experiments precisely in the range between 840°C
and near 680°C. A temperature recovery phenomenon
is found in the cooling curves from almost 60 s after
starting of cooling. Some discrepancies are observed in
between the experimental and simulated cooling curves
in the range of the temperature recovery. When the
latent heat is not considered, simulated curves do not
show the recovery phenomenon as shown in Fig. 4.
These results suggested that the temperature recovery is
due to the latent heat. The simulated and measured
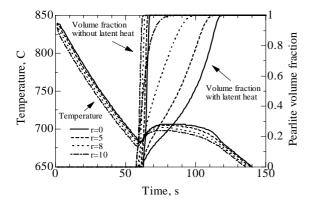temperature distributions during its recovery period are

Fig.6 Temperature and Pearlite Volume Fraction
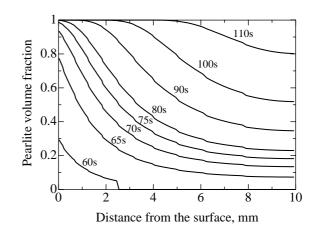Predictions in Air-Cooled Cylinder.

Fig.7 Simulated Distributions of Pearlite Volume
Fraction in Air-Cooled Cylinder.

shown in Fig. 5 for describing the effects by the latent
heat in detail.

Simulated temperature and volume fraction of
pearlite changes at four locations, 0 5, 8 and 10 mm
distances from the center as shown in Fig. 6. The
volume fraction change shows that the transformation
at the surface part progresses faster than that at the
center, although the temperature difference between the
center and surface of the cylinder is relatively small.
Ultimately, the transformation at the center can be seen
to occur almost 50 s longer than that at the surface.
When simulated without the latent heat, the volume
fraction curves at different locations are parallel for the
entire transformation period as shown in Fig. 6.

Agarwal et al. [9] reported the observation of this
transformation delay at the center, but did not offer an
explanation. This delay was explained by Arimoto et al.
[5] using locus curves on the plane of transformation
rate and temperature. They considered that the delay
occurs   because   of   both   the   high   temperature
dependency of the transformation activity and the
temperature difference due to latent heat, even if the
temperature difference between the surface and the
center is not large.

Simulated pearlite distribution changes during air-
cooling are shown in Fig. 7. Higher volume fractions of
pearlite are distributed near surface in the cooling range
between 60 and 110 s. The largest difference of the
volume fraction occurs between the surface and center
from 70 to 80 s. These results can be seen from the
curves of the volume fraction change at four locations
of the cylinder in Fig. 6.

In the tests, the specimens were initially cooled in air,
and finally quenched in the 5% brine solution. Since
brine quenching has high cooling ability, the retained
austenite in a specimen after the air-cooling would be
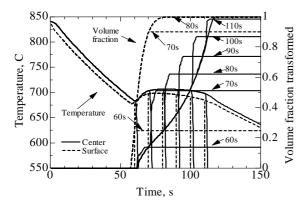almost   transformed   to   martensite,   and   the   pearlite

Fig.8 Temperature and Pearlite Volume Fraction Predictions in Air and Brine-Cooled Cylinder.

transformation may be stopped by the rapid cooling. It is suggested that the resulting pearlite distributions shown in Fig. 7 would be retained after brine quenching.

Figure 8 shows simulated temperature and volume fraction change in the cylinder during air and brine cooling. Six different times, 60, 70, 80, 90, 100 and 110 s for air-cooling were investigated. Once the brine quenching started, the pearlite transformation at the surface stops suddenly, while that at the center the process continues for a few seconds longer.

The experimental and predicted hardness distributions in the cylinder were compared as shown in Fig. 9. The hardness value h was calculated by the equation:

$$h = h_P \xi_P + h_M \xi_M \tag{3}$$

where ξ_P and ξ_M are the volume fraction of pearlite and maretensite, respectivly. h_P and h_M are the hardness for pearlite and martensite, 24 and 66 HRC, respectively, in this estimation.

The predicted and measured hardness exhibit similar distribution tendencies, which indicate inverse hardening for all cases. However, there were discrepancies in the magnitudes and timings. One reason for the discrepancies is most likely caused by the non-availability of TTT data for the steel specimens used in this research. It is believed that the process is extremely sensitive to minor differences in TTT data. In addition, the value of latent heat used in the simulations may not have been completely suitable for the bearing steels analyzed in the current work.

4. Conclusions

Experimental and simulated results were compared to verify the inverse quench-hardening phenomena in
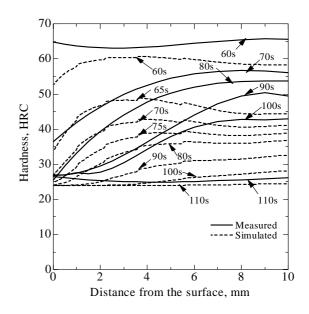

Fig.9 Experimental and Simulated Hardness Distributions in Specimens.

the specimens proposed by the pioneering work. The results obtained are summarized as follows:

(1) The predicted temperature recovery was found in the cooling curves of the specimen which produces the inverse quench-hardening phenomenon by the experiment.

(2) The inverse quench-hardening phenomena were verified from the experimental and simulated hardness distributions in the specimens.

(3) The test of the inverse quench-hardening in the cylinders can be applied for observing the pearlite transformation progress under the temperature recovery phenomenon during slow cooling.

(4) This experiment can be used for improving the accuracy in the model and data to describe the characteristics of the diffusion type transformation and its latent heat.

The thermal process simulator, FINAS/TPS, developed by CRC Solutions Corp. was used for the simulation in this research.

References

1   Shimizu N and Tamura I. Inverse Quench-hardening of Steel. Trans. ISIJ, 1976, 16: 655-663.
2   Shimizu N and Tamura I. Effect of Discontinuous Change in Cooling Rate during Continuous Cooling on Pearlitic Transformation Behavior of Steel. Trans. ISIJ, 1977, 17: 469-476.
3   Liscic B, Grubisic V and Totten G E. Inverse Hardness

Distribution and Its Influence on Mechanical Properties. In: Totten G E, Howes M A H, Sjostrom S J and Funatani K, Eds. Proceedings Second International Conference on Quenching and the Control of Distortion. Cleveland: ASM International, 1996, 47-54.

4   Liscic B and Totten G E. Benefits of Delayed Quenching. Advanced Materials & Processes, 1997, 9: 180-184.

5   Arimoto K, Huang D, Lambert D and Wu W T. Computer Prediction and Evaluation of Inverse Quench-Hardening of Steel. In: Funatani K and Totten G E, Eds. Proceedings of the 20th Heat Treating Conference. St. Louis: ASM International, 2000, 737-746.

6   Kolmogorov A N. Statistical Theory of Crystallization of Metals. Izvestia Akademii Naul SSSR, 1937, 1: 355-359.

7   Johnson W A and Mehl R F. Reaction Kinetics in Processes of Nucleation and Growth. Trans. AIME, 1939, 135: 416-458.

8   Avrami M. Kinetics of Phase Change. I, II and III. J. Chem. Phys., 1939, 7: 1103-1112, 1940, 8: 212-224, 1941, 9: 177-184.

9   Agarwal P K and Brimacombe J K. Mathematical Model of Heat Flow and Austenite-Pearlite Transformation in Eutectoid Carbon Steel Rods for Wire. Metall. Trans., 1981, 12B: 121-133.

10 Takeo K, Maeda K, Kamise T, Iwata H, Satomi Y and Nakata H. The Direct Patenting of High Carbon Steel Wire Rod by Film Boiling. Trans. ISIJ, 1975, 15: 422-428.

11 Guillermet A F and Gustafson P. An Assessment of the Thermodynamic Properties and the (p,T) Phase Diagram of Iron. High Temp.- High Press., 1985, 16: 591-610.

12 Awbery J H and Snow A. Total Heat at Various Temperature up to 950 C. In: Special Report No. 24, Iron and Steel Institute, 1939, 216-236.

13 Kramer J J, Pound G M and Mehl R F. The Free Energy of Formation and the Interfacial Enthalpy in Pearlite. Acta Metall., 1958, 6: 763-771.

14 Smith C S. A Simple Method of Thermal Analysis Permitting Quantitative Measurements of Specific and Latent Heats. Trans. AIME, 1940, 137: 236-245.

15 Krielaart G P, Brakman C M and Zwaag S Van Der. Analysis of Phase Transformation in Fe-C Alloys Using Differential Scanning Calorimetry. J. Mater, Sci.,1996, 31: 1501-1508.

16 Tajima M. The Effect of the Carbon Content on the Latent Heat of Phase Transformation of Iron and Steel. Tetsu-to-Hagane, 1998, 84(8): 7-12. (in Japanese)

17 US Steel. Atlas of Isothermal Transformation Diagrams. 1951, Pittsburgh.

18 The British Iron and Steel Research Association. Physical Constants of Some Commercial Steels at Elevated Temperatures. 1953, London: Butterworths Scientific Publications.

19 Miettinen J. Calculation of Solidification-Related Thermophysical Properties for Steels. Met. Mat. Trans. B, 1997, 28B: 281-297.

20 Yamaguchi T, Fukuei H, Shigematsu H and Harada K. Study on the Cooling Rate of Steel in Heat Treatment. Mitsubishi Juko Giho, 1969, 6(1): 30-39. (in Japanese)

Corresponding author: Mr. Kyozo Arimoto,
Email: arimo@arimotech.com,
Mail address: 822-10 Asonaka, Kaizuka, Osaka 597-0081 Japan,
Tel & Fax: +81-724-28-0272